



Full length article

Resolving the structure of organic nano strands self-assembled at a graphite-liquid interface using STM

Loji K. Thomas^{a,c,*}, Nadine Diek^b, Uwe Beginn^b, Michael Reichling^a^a *Fachbereich Physik, Universität Osnabrück, Barbarastr. 7, 49076 Osnabrück, Germany*^b *Institut für Chemie, Universität Osnabrück, Barbarastr. 7, 49076 Osnabrück, Germany*^c *Department of Physics, S.B College, Mahatma Gandhi University, Kerala, India*

ARTICLE INFO

Keywords:

STM
Self-assembly
Hydrogen bond
Strand
Solid-liquid interface
Graphite

ABSTRACT

Scanning tunneling microscopy (STM) at solution-graphite(0001) interface is used to identify nanometer-wide elementary strands of custom-designed amphiphilic benzamides and elucidate their internal structure with sub-molecular resolution. Evidences against graphitic artifacts that often mimic organic strands are provided, thereby unambiguously establishing the molecular origin of these strands. The aliphatic chain lengths are chosen based on bulk studies so as to promote strand architectures and avoid monolayer structures. Two different chain lengths are used to decipher the structural parameters and the results suggest hitherto unknown precursor routes to strand formation on a surface that is different from columnar mesophases in bulk. An on-surface self-assembly into hydrogen-bonded tetramer precursors and their subsequent interaction with other units via van der Waals forces between the dangling alkyl chains is proposed for strand formation on the surface.

1. Introduction

One-dimensional micro- and nano-structures of organic compounds are valuable ingredients in solution-processable organic electronic devices [1–5]. Electron transport through organic structures is the basis for a large number of biological processes as well [6]. Supramolecular self-assembly in solution is a strategy devised by nature to build larger functional ensembles [7]. Several synthetic low-molecular weight (LMW) wedge-shaped and amphiphilic 3,4,5-tris(alkoxy)benzamides are known to self-assemble into columnar mesophases in bulk [8], resulting in self-assembled fibrillar networks in non-polar and semi-polar solvents. Organogelators, due to their tendency to form nanostrands, have aroused much interest in the context of nanoelectronics [9]. It is imperative to decipher the structure of these nanostructures to identify the function they can perform such as their potential use as selective ion-transport channels.

The knowledge about columnar bulk mesophase materials mostly come from X-ray diffraction, scattering and electron microscopy techniques that generally suffice for a macroscopic understanding [10,11]. At a solid-liquid interface, the surface may also play a role in the molecular self-assembly process. Due to the possibility of on-surface organization of the molecules via non-covalent interactions, we could expect structures that may differ drastically from that in bulk. Further, self-assembly on surfaces might be influenced by other factors, for

instance, solution concentration, where denser polymorph usually results from higher solution concentrations [12,13]. The hydrophobic HOPG is an ideal substrate for the investigation of amide moieties-containing compounds such as the ones investigated here. In contrast, hydrophilic substrates, in general, may hinder [14–16] the self-assembling ability of the molecules by forcing them to lie flat on the surface, although deviation from this behavior has also been reported [17]. For a discussion on the influence of substrates on the self-assembly of fibril structures on HOPG and Au, see [18–21]. To elucidate structural details of self-assembled strands on HOPG, we use scanning tunneling microscopy (STM), the only available technique that can resolve structural details at the sub-molecular level.

STM is an efficient technique to probe the structure as well as reactivity in a chemically ‘realistic’ environment- that is at solid-liquid interfaces [22–36]. However, unlike planar surface structures [37,38], the realm of isolated 1-D structures such as nanowires, has been less exploited by this technique. STM imaging of 1-D structures has been successful in imaging films of closely packed strands, edge-on stacks [26,39–41] and innate graphitic structures [42–46], but only few reports of isolated organic strands are found [47–52]. This is mostly owing to difficulties in locating isolated, single-digit nanometer-wide wires on a millimeter-wide probe area, using an STM having a range of only few hundred nanometers. Due to the small size of strand entities compared to the total scan area, the nanostrands (i.e those with only

* Corresponding author at: Department of Physics, S.B College, Mahatma Gandhi University, Kerala, India.

E-mail address: lkphysicsb@gmail.com (L.K. Thomas).<https://doi.org/10.1016/j.apsusc.2019.03.072>

Received 23 December 2018; Received in revised form 17 February 2019; Accepted 8 March 2019

Available online 12 March 2019

0169-4332/ © 2019 Elsevier B.V. All rights reserved.

about 5 to 7 nm as reported here) appear invisible to optical microscopy or even AFM imaging. Therefore, AFM and optical microscopy were employed only to understand the large-scale morphology, and STM was the main technique used for locating as well as resolving the structural details. Other factors are thermal drift in ambient conditions, tip contamination and movement/perturbation of the strand (particularly for physisorbed entities) caused by tip motion [53,54]. Although vacuum and low-temperature conditions may offer some advantage here, for the sake of the dynamic chemistry involved, the ideal choice is the solid-liquid interface. With regard to STM imaging of linear objects on HOPG, an important aspect that one should be wary of is the innate graphitic artifacts seen on bare graphite(0001) surface [42–45] that show a strikingly close resemblance, mimicking the molecular strands. This, however, can still be distinguished, for example, by ensuring the absence of graphite steps or misoriented grain boundaries, absence of single/multiple steps near the molecular wires and the discrepancy in the reported periodicities of graphitic linear artifacts from that of adsorbate structures [42–45]. The aforementioned characterizes the primary causes for the existence of electronically induced ‘virtual’ periodic linear objects. Apart from these, in our study, we present strong evidences in support of the molecular origin of the strands such as confluence of strands leading to strand-bundles, scan-induced damage in strands, deviation from linear array of single strands and herringbone arrangement in multi-strands.

2. Experimental

2.1. STM/AFM imaging

Preparation of solutions and STM/AFM imaging: Varying solution concentrations of the compounds were prepared by dissolving in 1,2,4-trichlorobenzene ($C_6H_3Cl_3$, dielectric constant 2.2, boiling point 214 °C, 99% pure, Sigma-Aldrich Laborchemikalien GmbH, Seelze, Germany) in a dilution series in steps of 1/10. The solutions were sonicated or oven-heated to 45 to 50 °C for five to fifteen minutes prior to drop-casting on freshly cleaved highly oriented pyrolytic graphite (HOPG) (ZYB grade, SPI supplies, West Chester, PA, USA). Higher solution concentrations generally showed a gel phase, therefore in order to locate and image isolated strands by STM, a drop of the solvent was allowed to slide over the surface to avoid the formation of strand bundles or larger aggregates. STM images were taken in the constant current mode under ambient conditions with a compact STM (easyScan, Nanosurf AG, Liestal, Switzerland). Mechanically sharpened Pt/Ir 80/20% wires (Goodfellow Cambridge limited, Huntingdon, United Kingdom) were used as tips. Prior to measurements on molecular layers, the bare HOPG substrate was imaged to ensure the quality of the STM tip. By imaging the atomic structure of the bare graphite, the scanner was calibrated in regular time intervals so that the precision of measurement is solely limited by thermal drift. The ambient temperature was stabilized to be within ± 1.0 °C of room temperature and the scanner was always allowed time during measurements to thermally equilibrate and mechanically relax to reduce thermal drift and piezo creep to a minimum. Furthermore, images used for structural analysis were those with minimal thermal drift and a calibration was done with respect to the graphite lattice whenever possible. For imaging molecular structures, the tip was retracted slightly and a drop of the solution was applied onto the basal plane of HOPG to form a meniscus between the tip and the surface. Occasionally, another preparation method was used- a drop of the solution was drop-cast on HOPG prior to imaging. Imaging was performed at the solution-solid interface where typical operating conditions were $V_t = 1.3$ V (tunneling voltage) and $I_t = 0.60$ nA (tunneling current) for the molecule and 0.05 V at 1.00 nA for imaging the bare graphite substrate. Images represent raw data unless otherwise mentioned and flattening has been done only for large area images using the WSxM software [57]. A Nanosurf (Nanosurf AG, Liestal, Switzerland) AFM in contact-mode was used to characterize the

nanoscale morphology. Silicon cantilevers (Nanosensors) with force constants in the range 0.2–0.4 N/m were employed and the images were taken in ambient conditions at a scan frequency of 1–3 Hz with a typical set point of 25 mN. Topographic data were recorded simultaneously in trace and retrace to check for scan artifacts.

2.2. Synthesis and characterization

Materials- Ethyl 3,4,5-trihydroxybenzoate (96%, Fluka), 1-bromooctane (98%, Merck), 1-bromodecane (98%, Alfa Aesar), 1-bromododecane (97%, Aldrich), 1-bromotetradecane (98%, Alfa Aesar), ammonia solution 32% (30%, Merck), methyl 4-hydroxybenzoate (99%, Sigma Aldrich), methyl 3,4-dihydroxybenzoate (97% Alfa Aesar), potassium iodide (99.5%, Fluka), potassium carbonate (99%, Sigma Aldrich), potassium hydroxide (85–100%, Sigma Aldrich), hydrochloric acid (37%, Sigma Aldrich), thionylchloride (98%, Sigma Aldrich), hydrazine monohydrate (98%, Alfa Aesar).

Techniques- 1H NMR(500 MHz) and ^{13}C NMR(125 MHz) were measured on a Bruker Avance DPX-250 spectrometer, tetramethylsilane (TMS) was applied as internal standard in deuterated chloroform at 20 °C. melting points were measured on a Netzsch DSC 204 ‘Phoenix’ differential scanning calorimeter (DSC). About 10 mg of sample was used. In all cases, the heating and cooling rates were 10 °C/min. Indium and cyclohexane were used as calibration standards. IR spectra were measured on a “Bruker Vertex 70” FT infrared spectrometer, equipped with a “Golden Gate Diamond ATR reflection-device”. TLC has been performed on Silica gel 60 F₂₅₄ plates (Merck).

Synthesis of ethyl 3,4,5-tris(octyloxy)benzoate [1]: 19.817 g (100 mmol) ethyl 3,4,5-trihydroxybenzoate was dissolved in 500 ml cyclohexanone, 330 mmol 1-bromooctane, 330 mmol potassium carbonate and 0.5 g potassium iodide were added and heated under reflux for 5 h under a nitrogen atmosphere. The reaction mixture was filtered hot and concentrated on a rotary evaporator. After recrystallization from 600 ml MeOH/EtOH(2/1), a white wax-like solid was obtained. Yield: 39.1 g; 73.2% of theory. TLC (Petrolether:Ethylacetate = 96:4): $R_f = 0.72$. 1H NMR ($CDCl_3$ δ /ppm): 0.912 (T, 9H, $-CH_3$), 1.315 (M, 24H, $-CH_2-$), 1.383 (S, 3H, $-COO-CH_2-CH_3$) 1.502(M, 6H, $-CH_2-CH_2-CH_2-O$), 1.77 (M, 6H, $-CH_2-CH_2-O$), 4.04 (T, 6H, $-CH_2-O$), 4.37 (M, 2H, $-COO-CH_2-CH_3$) 7.29 (S, 2H, aromatic).

Synthesis of 3,4,5-tris(octyloxy)benzoic acid [2]: 26.74 g (50 mmol) of [1] was dissolved in 350 ml boiling EtOH, a solution of 11.2 g (200 mmol) KOH in 25 ml water was added and heated under reflux for 4 h. The reaction mixture was poured into 1 l dest. water, acidified with hydrochloric acid to pH 1 and stirred for 1 h. After the precipitate was filtered and recrystallized in Acetone; 18.38 g (72.6% of theory) of white crystals were obtained. TLC (Petrolether:Ethylacetate = 9:1): $R_f = 0.83$. 1H NMR (MeOD δ /ppm): 0.922 (T, 9H, $-CH_3$), 1.357 (M, 24H, $-CH_2-$), 1.522 (M, 6H, $-CH_2-CH_2-CH_2-O$), 1.73-1.82 (2M, 6H, $-CH_2-CH_2-O$), 4.03 (T, 6H, $-CH_2-O$), 7.3 (S, 2H, aromatic).

Synthesis of 3,4,5-tris(octyloxy)benzoyl chloride [3]: 10 g [2] was refluxed with 50 ml thionylchloride for 2 h. The solvent was evaporated in vacuum. Finally 6.9694 g (67.2% of theory) of white crystals were obtained after recrystallization in Acetone. TLC (Petrolether:Ethylacetate = 96:4): $R_f = 0.28$. 1H NMR ($CDCl_3$ δ /ppm): 0.851 (T, 9H, $-CH_3$), 1.3 (M, 24H, $-CH_2-$), 1.4 (M, 6H, $-CH_2-CH_2-CH_2-O$), 1.41 (M, 6H, $-CH_2-CH_2-O$), 3.969-4.060 (2T, 6H, $-CH_2-O$), 7.29 (S, 2H, aromatic).

Synthesis of 3,4,5-tris(octyloxy)benzamide [4] (3CB-8): 5.2529 g of [3] was dissolved in 20 ml dry dioxane, 5 ml conc. Ammoniac solution (32%) was added, and stirred at room temperature for 2 h then the mixture was poured into 100 ml water and neutralized with 20% hydrochloric acid and stirred for 30 min. The mixture was filtered and the precipitate recrystallized two times in EtOH. Yield: 3.94 06 g (77.9% of theory) of white, cotton-like crystals were obtained. DSC measurements: (1st run, 10 °C/min), melting temperature = 84.4 °C (lit. 82 °C). 1H NMR ($CDCl_3$ δ /ppm): 0.904 (T, 9H, $-CH_3$), 1.30 (M, 24H, $-CH_2-$), 1.45 (M, 6H, $-CH_2-CH_2-CH_2-O$), 1.76 (M, 6H, $-CH_2-CH_2-O$), 4.02 (T, 6H,

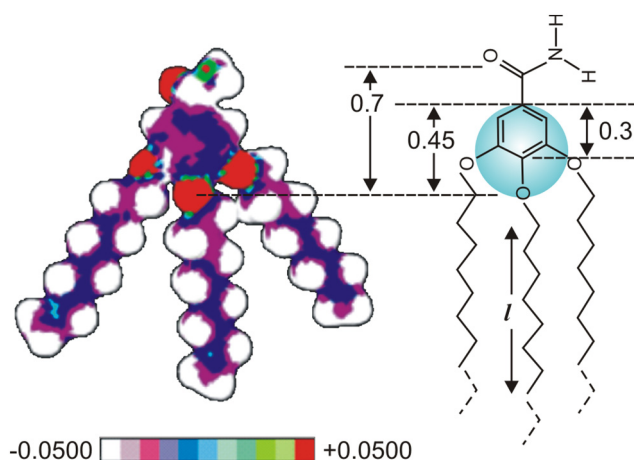


Fig. 1. (right) Structure and dimensions of 3CB- n with stretched alkyl chains; $n = 8$ (zig-zag line), and 10 (dotted line). Distances are in nm. ‘ l ’ represents the length of the aliphatic tails. (left) electrostatic potential (ESP) plot of 3CB-8. The red end of the color map represents the most negative (electron-rich) and the white end the most positive regions (S1). The ‘wedge-shape’ of the molecule is visualized as the head group constituting the wedge apex and alkyl chains forming the wedge tail.

(-CH₂-O-), 5.7 (broad, 2H, -NH₂), 7.02 (S, 2H, aromatic). ¹³C NMR (CDCl₃ δ /ppm): 14.00 (-CH₃), 22.82 (CH₃-CH₂-), 26.0–32 (Calkyl), 29.51 (-CH₂-CH₂-O-), 30.47 (-CH₂-CH₂-O-), 69.6, (-CH₂-O-) 76.9 (-CH₂-O-) 106.5 (C2), 128.33 (C1), 141.9 (C4), 153.26. [55–57]

3. Results and discussion

We study elementary strands formed at graphite(0001)-1,2,4-trichlorobenzene (1,2,4-TCB) interface from a custom-designed wedge-shaped amphiphilic compound namely 3,4,5-tris(alkoxy)benzamide (3CB- n ; $n = 8, 10$). Here “ n ” stands for the number of methylene units in the aliphatic chains. The dimension of the 3CB- n molecules with stretched alkyl chains is illustrated in Fig. 1. In general, the molecular geometry of the mesogens is decisive for the generation of columnar mesophases in bulk. For example, with cunic and discotic molecules, columnar phases are frequently observed [8,54,55]. 3CB- n with its wedge-shape is the simplest class of thermotropic mesogens that form supramolecular columnar phases. X-ray, enthalpy measurements and temperature dependent IR spectroscopy [8] have revealed 3CB-8 to exhibit a rectangular disordered phase (C_{rd}) [8,56]. The mesophase generation depends also on the number as well as the length of the alkyl chains. Three-chain 3CB- n with $n \leq 4$ produced a crystalline structure, 3CB-5 exhibited a monotropic phase and $n = 6$ –14 yielded an enantiotropic columnar phase. Longer alkyl chains ($n > 15$) were found to impede mesophase formation. In bulk, individual molecules are believed to first self-assemble into disc-shaped hydrogen-bonded dimers and subsequently stack up to form columns. We have chosen the chain lengths with $n = 8$ and 10, based on the bulk studies so as to avoid monolayer formation since longer chains may promote alkyl chain-graphite interaction that may hinder strand formation.

Initially we used AFM (Fig. 2) and optical microscopy (see also supplementary information S2 and S3) for revealing the large-scale morphology and to confirm the capability of the compounds to produce fibrillar entities on a surface. AFM images reveal that 3CB- n is capable of yielding strands with high aspect ratios on graphite(0001) as well as Au(111) surfaces- both hydrophobic, from solutions of both high (2.856 wt%- gel phase) as well as dilute (0.285 wt% or less) samples.

Before discussing the STM results, in view of the graphitic linear artifacts, it is imperative to unambiguously establish the molecular origin of these strands. There are two options: one is to do control experiments using STM and the second is to exclude artifacts in view of

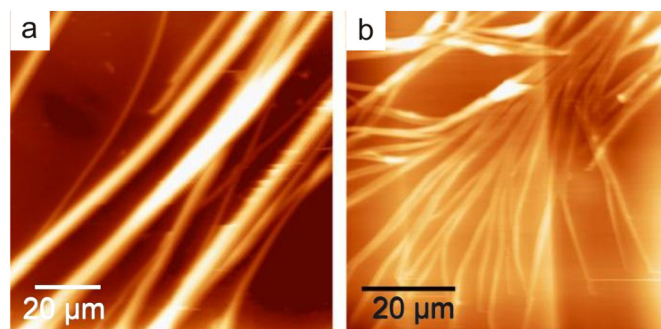


Fig. 2. AFM images in ambient conditions showing randomly oriented micrometer-wide strand bundles of 3CB-8 on (a) Au(111) and (b) graphite(0001) facets. Solution concentrations: (a) 2.856 wt% and (b) 0.285 wt%. More AFM images are available in supporting information (S2).

characteristics not peculiar of them. The control experiments, however, are best suited for extended adstructures on HOPG and not ideal for isolated single-digit nanometer-wide 1 D structures due to intrinsic limitations associated with STM imaging at solid-liquid interfaces. One of the control experiment is to image the bare surface first. This is also a routine procedure done to ensure the quality of the tip during STM imaging. However, this may not guarantee a verification of the presence or absence of graphite artifacts since it is known that the presence of a solvent/organic solution may facilitate or induce artifacts on HOPG [46]. That is, artifacts could be induced more easily after solution is drop cast on the surface (for example, a rotation of grains may be visualized by STM as a moiré superlattice (2D) or as a 1D entity (electronic) at the domain boundary). Further, for STM in solid-liquid environment, the tip has to be retracted back to drop cast molecules on the surface, and when approached again, the scan area may change by several micrometers. Thus, unlike planar films or films of strands extending over grain size of micrometer dimensions, control experiment is not a suitable solution. Same difficulties applies to a control experiment where the strands are removed from the surface after imaging them, and then imaging the same area to ensure the absence of these strands. The best way to remove the strands is to add solvent to the interface. This again is met with the same problems as in the first control experiment. In addition, usually this will result in an unstable imaging condition resulting in no further imaging possible with the same tip. Thus the control experiments using STM are not easy to perform in the case of sparsely populated isolated strands on a surface. Further, there are two types of linear artifacts on pristine HOPG- one is ‘real’ 1 D structure such as folding near a step edge, and a second type that are ‘virtual’ ones occurring due to electronic superposition. Due to these reasons, to establish the molecular origin of the strands, we resort to identifying the characteristics of the molecular strands that are distinct to them and not shown by graphitic artifacts. We have identified the following distinguishing features in the strands that could only be exhibited by molecular strands. In Fig. 3a, a confluence of few thin strands (see arrows) of 3CB-8 leading to the formation of a strand-bundle is visible where the orientation of individual strands as well as the bundle differ by $\sim 120^\circ$ influenced by the graphite symmetry. This fortuitous observation of thinner strands joining to form a bundle and their relative orientations represents a strong evidence for the molecular origin of these strands. Further, for isolated single strands, a deviation from the perfect linear array-type arrangement, as visible in Fig. 4b is observed. Such occurrence is highly unlikely for graphitic 1 D structures and has never been reported before [42–45]. This is understandable since perfect graphitic linear periodic structures result from electronic effects and they are not ‘real’ objects (except curved step edges or CNT type entities which are easily distinguishable). The easiest way to identify such virtual linear objects from real strands is to check for misoriented grains on either side of the linear entity, see for example

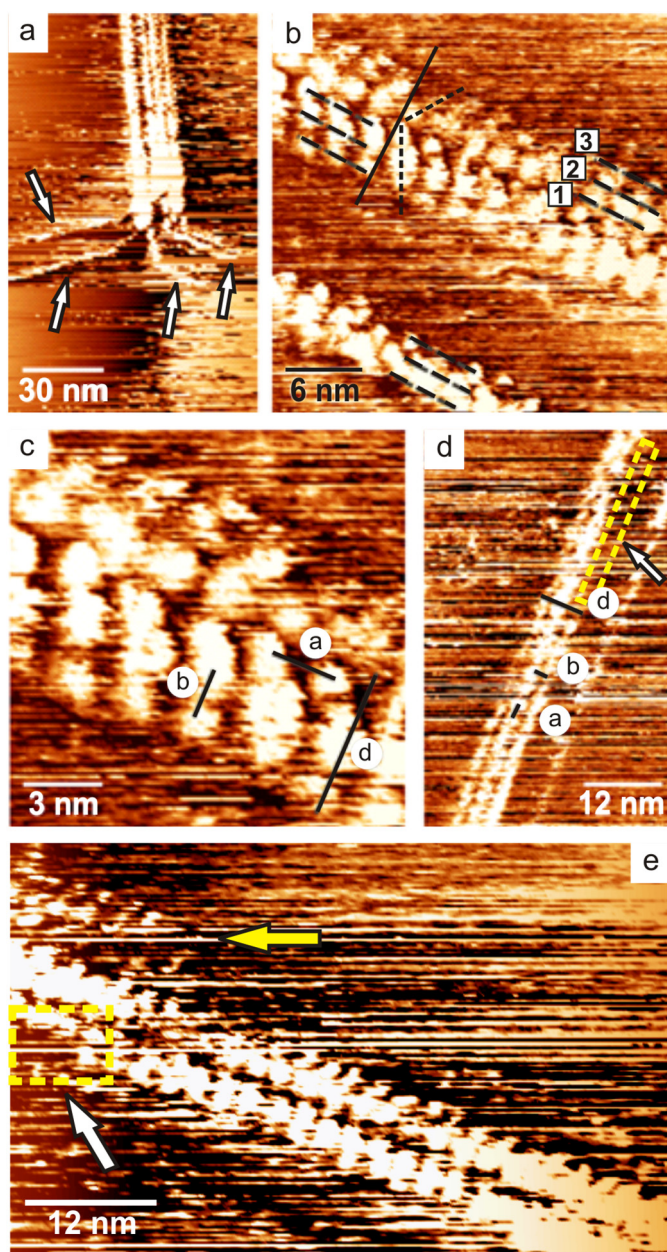


Fig. 3. Raw STM images of elementary strands of 3CB-8 self-assembled at 1,2,4-TCB-graphite(0001) interface after drop-casting from a 2.85 wt.-% solution. (a) confluence of thin strands lead to a strand-bundle, all individual strands as well as the bundle follow graphite lattice symmetry (b) three three-strands of 3CB-8, one isolated and two in proximity. (c) Linear parameters a , b and d of the three-strands of 3CB-8 and (d) that of 3CB-10 (concentration- 2.5 wt.-%). (e) Missing fragment (dotted rectangle) and damaged region along the fast-scan direction of the strands (yellow arrow). STM operating parameters are (a) 1.36 V, 0.6 nA; (b, c, e) 1.6 V, 0.6 nA; and (d) 1.09 V, 0.48 nA. The STM images are raw images and software processing was limited only to flattening.

supporting information S4(a). There are also strands found with missing fragments caused by tip motion at the solid-liquid interface as in Fig. 3d and e (see white arrows pointing to the dashed yellow rectangles) or scanning causing damage along the fast-scan direction washing away fragments from the strands (yellow arrow in Fig. 3e). These observations unambiguously exclude graphitic origin of these bright linear features. It can also be seen from literature [42–46] that graphitic multi-strands mostly appear with their bright blobs arranged in a side-by-side replica-type pattern perpendicular to the strand axis with no herringbone feature [42] in contrast to molecular nanowires [58] or

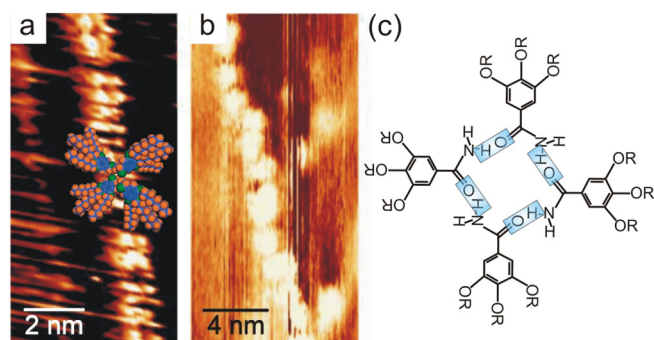


Fig. 4. STM images of single-strands of: (a) 3CB-8 (concentration- 0.57 wt.-%) and (b) 3CB-10 (concentration- 2.5 wt.-%). A space-fill model of a tetramer of 3CB-8 is superimposed roughly on the STM image in (a) where the aliphatic chains appear ‘dark’ in the STM image. A larger image of (a) is available in S5. (c) Schematic of a 3CB- n hydrogen-bonded cyclic tetramer formed from four 3CB- n molecules. The blue rectangles highlight the O–H bonds between 3CB- n molecules.

herringbone appearance as in Fig. 3. Note also that the blob arrangement represented by dashed lines in Fig. 3b in the two neighboring three-strands forms a zigzag that excludes any scan direction-dependence in STM imaging. These evidences collectively define the molecular origin of the strands reported in this article.

In order to elucidate the internal structure, locating thin strands becomes necessary and therefore, formation of thick strand bundles should be prevented. To obtain thin strands, we resorted to using only dilute solutions for STM studies. But this has the effect of producing fewer number of strands which then makes it difficult to locate strands on a 1 cm \times 1 cm HOPG surface using an STM having a range of about 700 nm. Also, unlike planar films [38,59], getting quality STM images of ‘real’ strands is often difficult (unlike electronically-induced ‘virtual’ graphitic artifacts). Based on the STM images, the nanoscale morphology of 3CB- n is seen to consist of a sparse population of thin strand bundles having widths of few tens of nanometers and elementary strands of only few nanometers (Fig. 3). Unlike the thick bundles (AFM images in Fig. 2) which remained stable for several hours to days; the elementary strands were easily perturbed by the raster scanning of STM imaging in the fast scan direction (Fig. 3e). We have found two types of elementary strands: some consisting of a three-strand geometry (Fig. 3b,c,d) and some with single-strand appearance (Fig. 4a,b). Amongst these, the three-strands (represented by three black dotted lines named 1,2, and 3 in Fig. 3b) were the most frequently observed strand type- for both 3CB-8 as well as the longer chain counterpart 3CB-10; while single-strands were seldom seen. Fig. 3b shows three-strands of 3CB-8, one isolated and two others lying in close proximity while Fig. 3d is a three-strand of 3CB-10. Thin bundles as well as the elementary single-strands and three-strands are seen to always align along one of the two graphite crystallographic directions namely $\langle 11\bar{2}0 \rangle$ $\langle 01\bar{1}0 \rangle$ (S4). The aliphatic chains, as usual, are not visible in the STM images and may be assigned to the dark region in between the bright blobs [38]. The orientation of the strands on HOPG could be attributed to CH- π interactions between the chains and the graphite surface in analogy with simple alkanes [60,61], or liquid crystalline mesogens [62–64].

The linear parameters of the elementary strands are given in Table 1. The chemical structure of 3CB-10 differs from 3CB-8 only by two methylene units resulting in a difference in their chain lengths (Δl) of 0.25 nm (Fig. 1). The repeat distance/periodicity (a) (Fig. 3c) of the three-strands of 3CB-10 along the strand axis, however, show a reduction by ≈ 0.6 nm from that of 3CB-8 strands, while the lateral inter-strand separation (b) increases by ≈ 0.7 nm. Thus the variations in these parameters are proportional by about twice the increase in chain length Δl . Now the width of the three-strands of 3CB-10 is larger by ≈ 1.7 nm

Table 1
Linear dimensions (nm) of the three-strands and single-strands of 3CB-*n* (*n* = 8,10).

	3CB-8	3CB-10
Chain length <i>l</i>	0.87	1.12
Three-strand		
Periodicity <i>a</i>	2.6 ± 0.1	2.0 ± 0.2
separation <i>b</i>	1.8 ± 0.1	2.5 ± 0.2
Diameter <i>d</i>	5.1 ± 0.2	6.8 ± 0.1
Single-strand		
Periodicity <i>a</i>	2.0	1.55
Diameter <i>d</i>	1.4	1.4

that is in agreement with twice the increase in inter-strand separation ($\approx 2 \times 0.7$ nm). In short, the increase in chain length is immediately manifested as an increase in the intra- and inter-strand separations. Because the only difference between 3CB-8 and 3CB-10 is in the length of their aliphatic chains, we assign the dark regions, i.e. the inter-strand separation, between the bright blobs in the STM images to the presence of alkyl chains [38,65]. Therefore, it seems possible that the longer chain of 3CB-10 essentially increases the interdigitation between the chains along the strand axis resulting in pulling the bright blobs closer (i.e. results in a reduced *a*), but this simultaneously effects a relaxation in the lateral direction causing *b* to increase. A similar reduction in *a* of ≈ 0.45 nm was observed between the single-strands of 3CB-8 and 3CB-10 (Fig. 4 and S5), again about twice the increase in chain length Δl . This in turn implies that the aliphatic chains play a role in the interactions between the bright blobs in the STM images presumably via van der Waals (vdW) forces. Note also that, due to lack of sufficient van der Waals forces from all directions, the isolated single strands may appear less linearly ordered than their three-strand counterparts (Fig. 4b) unless they lie close to a thicker bundle (S5). The bright blobs in the three-strand of 3CB-*n* possess a diameter of 1.56 ± 0.21 nm, while single strands of 3CB-*n* consists of bright blobs of ~ 1.4 nm, which occasionally can be further resolved to be consisting of four smaller lobes of size ≈ 0.4 – 0.5 nm with a dark spot at the center (S5). The aromatic core of the molecule has a higher electron density due to the delocalized orbitals, and is expected to be observed as a bright region in STM images compared to the sigma-bonded aliphatic chains that usually appear dark [63]. In order to understand the origin of bright blobs in the STM image, frontier molecular orbitals (MO's) and the electrostatic potential (ESP) [66] of 3CB-8 were plotted (see S1) using *ArgusLab* [67]. No similarities to MO's were found. ESP is a concept recently explored for interpretation of STM images of physisorbed molecules [68]. The ESP plot for 3CB-8 is shown in Fig. 1 with regions relatively rich in electrons color mapped at the red end. With reference to this map, the small bright blobs appearing in the STM images (≈ 0.45 nm) could be assigned to the aromatic core plus the oxygen atoms (blue shaded circle in the skeletal model of 3CB-*n* in Fig. 1). Based on the above parameters obtained from STM measurements, we speculate that a bright blob (of 1.56 nm) in the STM image could be assigned to the central core of a 3CB-*n* tetramer whereas the aliphatic chains appear dark.

For supramolecular self-assembly on the surface, 3CB-*n* is bestowed with amide functionalities that could facilitate intermolecular hydrogen bonding [40] and alkyl chains that could promote physisorption on the graphite surface through CH- π interactions as well as inter-chain vdW interaction [69–74]. It should be emphasized that the length of the alkyl chain is so chosen to produce strand architectures on the surface [8,56]. Therefore, to avoid monolayer formation of flat-lying molecules, we limit the chain length to *n* = 8 and 10. Note that the benzamides in their gas phase exhibit a rotation of the amide group by 26° with the plane of the aromatic ring [75], which may further facilitate tetramer formation on the surface even with one or more of the alkyl chains of 3CB-*n* still attached to the surface. If a molecule of 3CB-*n* gets

adsorbed on the surface, then through hydrogen bonding with other molecules via their amide moieties, a tetramer could be formed on the surface. Due to this anchoring of molecules on the surface, a tetramer could formed more easily on a surface than in solution. Thus the tetramer formation, in this case, might essentially be a surface-supported process. This could be the reason why the strands are aligned along graphite axes. The schematic of hydrogen-bonding in the tetramer configuration is shown in Fig. 4c (also see S6). A single strand could simply be an array of such tetramers on the surface when tetramers adsorbed on the surface interact via their dangling alkyl chains. A space-fill model of a 3CB-*n* tetramer is superimposed on Fig. 4a. The single strands adsorbed on the surface could act as an anchoring unit for the formation of multi-strands via non-covalent interactions. The question remains why the most common adstructure is the three-strand geometry and why no extended monolayer is formed? This is presumably due to the fact that a 'flat' orientation of the molecule due to surface-molecule interaction (S7) is possible only when these forces exceeds inter-molecular interactions. With three alkyl chains per molecule, a monolayer formation is unlikely due to their interaction with other tetramers/strands in the supernatant, that may 'raise' the strands away from the surface. That is, the molecules/strands may be pulled away from the surface and possibly minimize their energy by evolving into a more curved geometrical structure.

The formation of a three-strand does not seem to be a simple juxtaposition of single-strands arranged side-by-side on the surface (otherwise it will lead to a monolayer of face-on molecules), but may include an optimization of the geometry and energy due to all non-covalent interactions at play. One hint about this comes from the apparent height of individual strands in a three-strand (Fig. 5b) and those in thin strand bundles (Fig. 5a). The apparent height of strands vary between 0.4 nm to 0.9 nm (height profile of 3CB-10 is given in S8). Besides, the presence of twelve alkyl chains per every tetramer is a highly favorable factor for inter-strand van der Waals interactions. This, is strictly applicable only to the central strand since the side chains of the lateral strands may get attached to the surface. Note the herring-bone arrangement in three-strands where a bright blob from one strand is placed in a perfectly appropriate position near the dark region of the neighboring strand, allowing interaction between the chains (Fig. 3c). Thus it is possible that the three-strands result from a spontaneous optimization of all possible intermolecular interactions between single

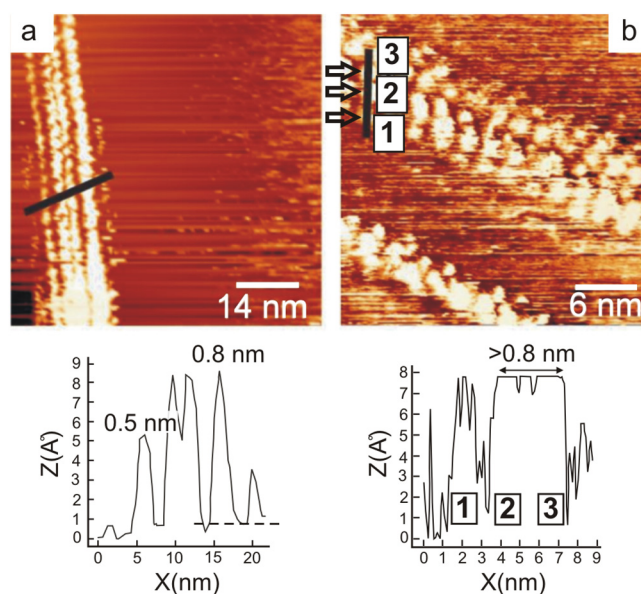


Fig. 5. Height profiles taken along the black lines in the STM images: (a) 3CB-8 strand bundle shown in Fig. 3a. (b) three-strands of 3CB-8. Tunneling parameters: ~ 1.36 V and 0.6 nA.

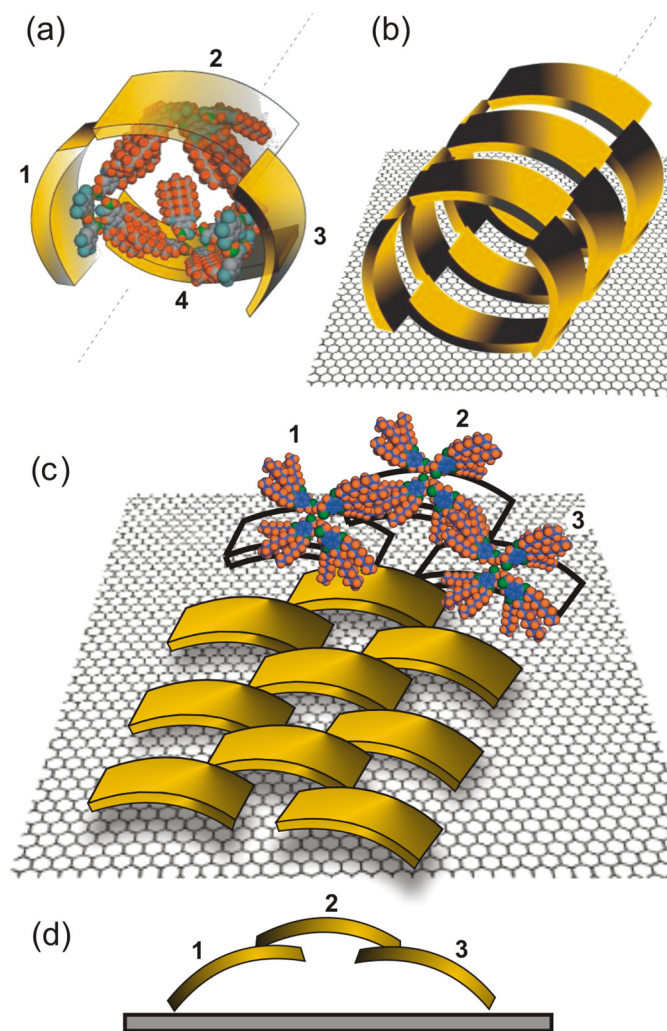


Fig. 6. Schematic of proposed models for the elementary three-strand structure of 3CB-*n* on HOPG: (a, b) model I with a repeat unit consisting of four tetramer motifs named 1, 2, 3 and 4 (front alkyl chains from tetramers 1 and 3 are omitted for clarity); (c) model II consisting of a basic structural unit with only three tetramer units which is more ‘flat’ than model I. (d) Cross-sectional view of model II.

strands.

Most noticeably, the periodicity a is much larger than the inter-stack distance of 0.35 nm observed in mesophase columns in bulk [10,11] or column arrays (edge-on stacks) on a surface [26]. This means that the strand structure cannot be explained by interactions stabilized by π^* orbital overlap of stacked aromatic rings. Therefore, on the surface, a different kind of mechanism must be involved. Since STM is the only available technique that can give finer structural details at the atomic or molecular level as pertinent to the situation here, and since the strands seem to result from an on-surface self-assembly, we solely limit our proposed models based on parameters obtained from STM images. We propose two tentative structural models for the three-strand structure of 3CB-*n* self-assembled on HOPG. In both models, the precursor is a tetramer represented as a curved rectangular block as illustrated in Fig. 6. Thus, the first step is the formation of tetramers via on-surface self-assembly followed by self-assembly into a herringbone pattern due to van der Waals bonding with other strands/tetramers.

In model I, the strands adsorbed on the surface, due to optimization of all non-covalent interactions, adopts a four-tetramer ring structure as the repeat unit that is a highly symmetric unit with the tetramer aryl cores arranged as shown in Fig. 6a, where tetramers marked 1 and 3 are

displaced along the strand axis by half the periodicity. There are 48 alkyl chains in each ring unit that are available for bonding to other strands which is a compelling factor to not to discard this model. Due to the symmetry of the ring unit, the dangling alkyl chains are at the right positions to connect to alkyl chains of a following ring. Hence, a string of four tetramer units constitute a repeat unit of the three-strand (Fig. 6b) with a well-defined diameter and a saturation of all possible van der Waals interactions between dangling alkyl chains. In the STM image, this arrangement will appear as a linear herringbone pattern (Fig. 3c). This model, nevertheless, cannot strictly adhere to the apparent height results from STM images. The apparent height in STM images, however, is not a clear indicator of the ‘true’ height since, in general, it represents a convolution of both topographic and electronic effects. Also the large number of alkyl chains available for lateral interactions may aid in forming more closed tube-like structures as shown. Due to these reasons, model I cannot be completely discarded, although it is less likely.

A more plausible arrangement is model II which is compatible with the height measurements from the STM images where the apparent height of the strands suggest a more ‘flat’ structure on the surface than model 1. The repeat unit here consists only of three tetramers as shown in Fig. 6c and d, where there is no closure into a tube-like geometry. Here the on-surface self-assembly into tetramers and then into single strands progresses as in model 1. Further interaction between strands leads to a three-strand structure as shown in Fig. 6c. In this case, the aliphatic chains of the two side strands are attached to the graphite surface while the chains of the central strand are fully engaged in van der Waals interaction with the tetramers of the side strands and not attached to the surface (Fig. 6d). Thus in STM images, the central strands possess a higher apparent height.

In both the models, it is evident that the ability to form a tetramer precursor is crucial. A different oligomer precursor, for ex. a dimer, might drastically change the strand structure. Tetramer, rather than dimer is favored on the surface whereas in the absence of a surface or in solution, a dimer may be preferred [8,76]. Thus the influence of surface in the supramolecular self-assembly process leading to the formation of strands is evident. It is easy to note that a more blunt wedge apex (for example with the head group NH-NH₂) may possibly hinder tetramer formation. That is, on a surface, the molecular shape may also affect the self-assembly onto the type of precursor that could be formed which ultimately decides the geometry and structure of the strand. In view of this, our on-going studies focus on other derivatives of 3CB-*n* with alterations both at the wedge apex (head group) and wedge tail (alkyl chains).

4. Conclusion

Using STM, we presented a molecular-scale characterization of the elementary organic strands formed through self-assembly of custom-designed wedge-shaped amphiphilic compounds namely 3,4,5-tris(alkoxy)benzamides at a graphite-1,2,4 TCB interface. In accordance with parameters deduced from the STM images, we proposed plausible structural models for the strands based on an on-surface self-assembly into tetramer precursors. The surface-support and the wedge-shape of 3CB-*n* allows for hydrogen-bonding between the amide moieties that may yield tetramers on the surface. The single-strand and three-strand structure results from tetramer strings inter-locked via van der Waals interactions between their dangling aliphatic chains.

Acknowledgements

This work has been supported by the Promotionsprogramm ‘Synthesis and Characterization of surfaces and Interfaces assembled from Clusters and Molecules’ funded by the State Government of Niedersachsen, Germany.

Appendix A. Supplementary data

Supporting material includes AFM and optical microscopy images, height profiles, basic simulation, MO and ESP plots. Supplementary data to this article can be found online at doi:<https://doi.org/10.1016/j.apsusc.2019.03.072>.

References

- [1] J.P. Hong, M.C. Um, S.R. Nam, J.I. Hong, S. Lee, Organic single-nanofiber transistors from organogels, *Chem. Commun.* (2009) 310–312.
- [2] A. Schenning, E.W. Meijer, Supramolecular electronics; nanowires from self-assembled pi-conjugated systems, *Chem. Commun.* (2005) 3245–3258.
- [3] L. Schmidt-Mende, A. Fechtenkötter, K. Müllen, E. Moons, R.H. Friend, J.D. MacKenzie, Self-organized discotic liquid crystals for high-efficiency organic photovoltaics, *Science* 293 (2001) 1119–1122.
- [4] J.L. Li, B. Yuan, X.Y. Liu, H.Y. Xu, Microengineering of supramolecular soft materials by design of the crystalline fiber networks, *Cryst. Growth Des.* 10 (2010) 2699–2706.
- [5] M. Hamed, A. Herland, R.H. Karlsson, O. Inganäs, Electrochemical devices made from conducting nanowire networks self-assembled from amyloid fibrils and alkoxysulfonate PEDOT, *Nano Lett.* 8 (2008) 1736–1740.
- [6] J.M. Ward, Z.M. Pei, J.I. Schroeder, Roles of ion channels in initiation of signal transduction in higher plants, *Plant Cell* 7 (1995) 833–844.
- [7] J. Otsuki, S. Eitaki, Y. Sei, K. Yamaguchi, Supramolecular fibers and microbelts from a phthalhydrazide derivative of crown ether with alkyl chains, *Chem. Lett.* 35 (2006) 1256–1257.
- [8] U. Beginn, Thermotropic columnar mesophases from N-H...O, and N...H-O hydrogen bond supramolecular mesophases, *Prog. Polym. Sci.*, 28 (2003) 1049–1105.
- [9] A.R. Hirst, B. Escuder, J.F. Miravet, D.K. Smith, High-tech applications of self-assembling supramolecular nanostructured gel-phase materials: from regenerative medicine to electronic devices, *Angew. Chem. Int. Ed.* 47 (2008) 8002–8018.
- [10] N. Boden, R.J. Bushby, J. Clements, B. Movaghar, K.J. Donovan, T. Kreuzis, Mechanism of charge transport in discotic liquid crystals, *Phys. Rev. B* 52 (1995) 13274–13280.
- [11] T.-Q. Nguyen, R. Martel, M. Bushey, P. Avouris, A. Carlsen, C. Nuckolls, L. Brus, Self-assembly of 1-D organic semiconductor nanostructures, *Phys. Chem. Chem. Phys.* 9 (2007) 1515–1532.
- [12] H. Wettach, S. Hoeger, D. Chaudhuri, J.M. Lupton, F. Liu, E.M. Lupton, S. Tretiak, G. Wang, M. Li, S. De Feyter, S. Fischer, S. Foerster, Synthesis and properties of a triphenylene-butadiynylene macrocycle, *J. Mater. Chem.* 21 (2011) 1404–1415.
- [13] C.A. Palma, J. Bjork, M. Bonini, M.S. Dyer, A. Llanes-Pallas, D. Bonifazi, M. Persson, P. Samori, Tailoring bicomponent supramolecular nanoporous networks: phase segregation, polymorphism, and glasses at the solid-liquid interface, *J. Am. Chem. Soc.* 131 (2009) 13062–13071.
- [14] I.A. Aksay, M. Trau, S. Manne, I. Honma, N. Yao, L. Zhou, P. Fenter, P.M. Eisenberger, S.M. Gruner, Biomimetic pathways for assembling inorganic thin films, *Science* 273 (1996) 892–898.
- [15] Y.J. Zhang, M. Jin, R. Lu, Y.L. Song, L. Jiang, Y.Y. Zhao, T.J. Li, Interfacial-dependent morphologies in the self-organization system of chiral molecules observed by atomic force microscopy, *J. Phys. Chem. B* 106 (2002) 1960–1967.
- [16] G.A. Ozin, A.C. Arsenault, L. Cademartiri, *Nanochemistry: a chemical approach to nanomaterials*, Royal Society of Chemistry: Cambridge, U.K., 2009; pp 530–531.
- [17] R. Rai, A. Saxena, A. Ohira, M. Fujiki, Programmed hyperhelical supramolecular assembly of nickel phthalocyanine bearing enantiopure 1-(p-tolyl)ethylamino-carbonyl groups, *Langmuir* 21 (2005) 3957–3962.
- [18] K. Perronet, F. Charra, Influence of molecular-substrate interaction on the self-assembly of discotic liquid crystals, *Surf. Sci.* 551 (2004) 213–218.
- [19] H.T. Jung, S.O. Kim, Y.K. Ko, D.K. Yoon, S.D. Hudson, V. Percec, M.N. Holerca, W.D. Cho, P.E. Mosier, Surface order in thin films of self-assembled columnar liquid crystals, *Macromolecules* 35 (2002) 3717–3721.
- [20] G. Henn, M. Stamm, H. Poths, M. Rucker, J.P. Rabe, Influence of order in thin smectic polymer films on the structure at the surface, *Physica B* 221 (1996) 174–184.
- [21] D.B. Amabilino, J. Puigmarti-Luis, Gels as a soft matter route to conducting nanostructured organic and composite materials, *Soft Matter* 6 (2010) 1605–1612.
- [22] S. De Feyter, F.C. De Schryver, Self-assembly at the liquid/solid interface: STM reveals, *J. Phys. Chem. B* 109 (2005) 4290–4302.
- [23] D. den Boer, T. Habets, M.J.J. Coenen, M. van der Maas, T.P.J. Peters, M.J. Crossley, T. Khoury, A.E. Rowan, R.J.M. Nolte, S. Speller, J.A.A.W. Elemans, Controlled templating of porphyrins by a molecular command layer, *Langmuir* 27 (2011) 2644–2651.
- [24] D. den Boer, M. Li, T. Habets, P. Iavicoli, A.E. Rowan, R.J.M. Nolte, S. Speller, D.B. Amabilino, S. De Feyter, J. Elemans, Detection of different oxidation states of individual manganese porphyrins during their reaction with oxygen at a solid/liquid interface, *Nat. Chem.* 5 (2013) 621–627.
- [25] J. Elemans, S. De Feyter, Structure and function revealed with submolecular resolution at the liquid-solid interface, *Soft Matter* 5 (2009) 721–735.
- [26] J. Elemans, M.C. Lensen, J.W. Gerritsen, H. van Kempen, S. Speller, R.J.M. Nolte, A. E. Rowan, Scanning probe studies of porphyrin assemblies and their supramolecular manipulation at a solid-liquid interface, *Adv. Mater.*, 15 (2003) 2070–+.
- [27] J. Elemans, R. Van Hameren, R.J.M. Nolte, A.E. Rowan, Molecular materials by self-assembly of porphyrins, phthalocyanines, and perylenes, *Adv. Mater.* 18 (2006) 1251–1266.
- [28] J.A.A.W. Elemans, E.J.A. Bijsterveld, A.E. Rowan, R.J.M. Nolte, Manganese porphyrin hosts as epoxidation catalysts - activity and stability control by axial ligand effects, *Eur. J. Org. Chem.* (2007) 751–757.
- [29] J.A.A.W. Elemans, S.J. Wezenberg, M.J.J. Coenen, E.C. Escudero-Adan, J. Benet-Buchholz, D. den Boer, S. Speller, A.W. Kleij, S. De Feyter, Axial ligand control over monolayer and bilayer formation of metal-salophens at the liquid-solid interface, *Chem. Commun.* 46 (2010) 2548–2550.
- [30] B. Hulsken, R. Van Hameren, J.W. Gerritsen, T. Khoury, P. Thordarson, M.J. Crossley, A.E. Rowan, R.J.M. Nolte, J.A.A.W. Elemans, S. Speller, Real-time single-molecule imaging of oxidation catalysis at a liquid-solid interface, *Nat. Nanotechnol.* 2 (2007) 285–289.
- [31] S. De Feyter, A. Gesquière, M.M. Abdel-Mottaleb, P.C.M. Grim, F.C. De Schryver, C. Meiners, M. Sieffert, S. Valiyaveetil, K. Müllen, Scanning tunneling microscopy: a unique tool in the study of chirality, dynamics, and reactivity in physisorbed organic monolayers, *Acc. Chem. Res.* 33 (2000) 520–531.
- [32] S. De Feyter, H. Uji-i, W. Mamdough, A. Miura, J. Zhang, P. Jonkheijm, A. Schenning, E.W. Meijer, Z. Chen, F. Wurthner, N. Schuurmans, J. van Esch, B.L. Feringa, A.E. Dulcey, V. Percec, F.C. De Schryver, Supramolecular chemistry at the liquid/solid interface probed by scanning tunneling microscopy, *Int. J. Nanotechnol.* 3 (2006) 462–479.
- [33] S. Lei, J. Puigmarti-Luis, A. Minoia, M. Van der Auweraer, C. Rovira, R. Lazzaroni, D.B. Amabilino, S. De Feyter, Bottom-up assembly of high density molecular nanowire cross junctions at a solid/liquid interface, *Chem. Commun.* 2008 (2008) 703–705.
- [34] M. Hibino, A. Sumi, I. Hatta, Scanning tunneling microscopy study on dynamic structural formation in mixed fatty-acid monolayers at liquid/graphite interface, *Thin Solid Films* 282 (1996) 594–597.
- [35] M. Hibino, Adsorption behaviors of mixed monolayers of n-alkanes at the liquid-solid interface, *Langmuir* 32 (2016) 4705–4709.
- [36] S. Lei, K. Tahara, F.C. De Schryver, M. Van der Auweraer, Y. Tobe, S. De Feyter, One building block, two different supramolecular surface-confined patterns: concentration in control at the solid-liquid interface, *Angew. Chem. Int. Ed.* 47 (2008) 2964–2968.
- [37] M. Lackinger, S. Griessl, W.A. Heckl, M. Hietschold, G.W. Flynn, Self-assembly of trimesic acid at the liquid-solid interface - a study of solvent-induced polymorphism, *Langmuir* 21 (2005) 4984–4988.
- [38] L.K. Thomas, A. Kühnle, S. Rode, U. Beginn, M. Reichling, Monolayer structure of arachidic acid on graphite, *J. Phys. Chem. C* 114 (2010) 18919–18924.
- [39] Y. Yang, Z.Y. Yang, Y.P. Yi, J.F. Xiang, C.F. Chen, L.J. Wan, Z.G. Shuai, Helical molecular duplex strands: multiple hydrogen-bond-mediated assembly of self-complementary oligomeric hydrazide derivatives, *J. Org. Chem.* 72 (2007) 4936–4946.
- [40] M. Yu, N. Kalashnyk, W. Xu, R. Barattin, Y. Benjalal, E. Laegsgaard, I. Stensgaard, M. Hliwa, X. Bouju, A. Gourdon, C. Joachim, F. Besenbacher, T.R. Linderorth, Supramolecular architectures on surfaces formed through hydrogen bonding optimized in three dimensions, *ACS Nano* 4 (2010) 4097–4109.
- [41] A. Schiffrin, A. Riemann, W. Auwärter, Y. Pennec, A. Weber-Bargioni, D. Cvetko, A. Cossaro, A. Morgante, J.V. Barth, Zwitterionic self-assembly of L-methionine nanogratings on the Ag(111) surface, *PNAS* 104 (2007) 5279–5284.
- [42] H.P. Chang, A.J. Bard, Observation and characterization by scanning tunneling microscopy of structures generated by cleaving highly oriented pyrolytic graphite, *Langmuir* 7 (1991) 1143–1153.
- [43] W.M. Heckl, G. Binnig, Domain-walls on graphite mimic DNA, *Ultramicroscopy* 42 (1992) 1073–1078.
- [44] P. Simonin, C. Goffaux, P.A. Thiry, L.P. Biro, P. Lambin, V. Meunier, STM study of a grain boundary in graphite, *Surf. Sci.* 511 (2002) 319–322.
- [45] C.R. Clemmer, T.P. Beebe, Graphite: a mimic for DNA and other biomolecules in scanning tunneling microscope studies, *Science* 251 (1991) 640–642.
- [46] Y. Wang, Y. Ye, K. Wu, Simultaneous observation of the triangular and honeycomb structures on highly oriented pyrolytic graphite at room temperature: an STM study, *Surf. Sci.* 600 (2006) 729–734.
- [47] D.L. Carroll, R. Czerw, D. Tekleab, D.W. Smith, Anomalous periodic structure of polypropylene chains observed with scanning tunneling microscopy, *Langmuir* 16 (2000) 3574–3577.
- [48] K. Petukhov, M.S. Alam, H. Rupp, S. Strömsdörfer, P. Müller, A. Scheurer, R.W. Saalfrank, J. Kortus, A. Postnikov, M. Ruben, L.K. Thompson, J.M. Lehn, STM spectroscopy of magnetic molecules, *Coord. Chem. Rev.* 253 (2009) 2387–2398.
- [49] D.D.D. Ma, C.S. Lee, F.C.K. Au, S.Y. Tong, S.T. Lee, Small-diameter silicon nanowire surfaces, *Science* 299 (2003) 1874–1877.
- [50] M.S. Alam, M. Stocker, K. Gieb, P. Müller, M. Haryono, K. Student, A. Grohmann, Spin-state patterns in surface-grafted beads of iron(II) complexes, *Angew. Chem. Int. Ed.* 49 (2010) 1159–1163.
- [51] N.V. Fischer, M.S. Alam, I. Jum'ah, M. Stocker, N. Fritsch, V. Dremov, F.W. Heinemann, N. Buzlaff, P. Müller, trans-1,2-Bis(N-methylimidazol-2-yl)ethylene: towards building blocks for 2D fabrics and MML-type 1D molecular strands, *Chemistry – A European Journal*, 17 (2011) 9293–9297.
- [52] N.V. Fischer, U. Mitra, K.-G. Warnick, V. Dremov, M. Stocker, T. Wölfle, W. Hieringer, F.W. Heinemann, N. Buzlaff, A. Görling, P. Müller, High resolution scanning tunneling microscopy of a 1D Coordination polymer with imidazole-based N,N,O ligands on HOPG, *Chem. Eur. J.*, 20 (2014) 11863–11869.
- [53] C. Rettig, M. Bödecker, H. Hövel, Carbon-nanotubes on graphite: alignment of lattice structure, *J. Phys. D* 36 (2003) 818–822.
- [54] L.L. del Mercato, P.P. Pomba, G. Maruccio, A. Della Torre, S. Sabella, A.M. Tamburro, R. Cingolani, R. Rinaldi, Charge transport and intrinsic fluorescence in amyloid-like fibrils, *PNAS* 104 (2007) 18019–18024.

- [55] H. Zschke, K. Nitsche, H. Schubert, Kristallin-flüssige 3,6-diphenyl-1,2,4-triazine, *J. Prakt. Chem.* 319 (1977) 475–484.
- [56] M. Parra, J. Belmar, H. Zunza, C. Zuniga, S. Villouta, R. Martinez, Synthesis of amides derived from 1, 3, 4-thiadiazole as mesogenic unit, *Bol. Soc. Chil. Quim.* 38 (1993) 325–330.
- [57] R.J. Twieg, Liquid crystals derived from semifluorinated alkoxybenzoyl hydrazines Au - Khairuddean, Melati, *Mol. Cryst. Liq. Cryst.* 503 (2009) 3–31.
- [58] Y. Lei, W.P. Cai, G. Wilde, Highly ordered nanostructures with tunable size, shape and properties: a new way to surface nano-patterning using ultra-thin alumina masks, *Prog. Mater. Sci.* 52 (2007) 465–539.
- [59] M. Lackinger, T. Muller, T.G. Gopakumar, F. Muller, M. Hietschold, G.W. Flynn, Tunneling voltage polarity dependent submolecular contrast of naphthalocyanine on graphite. A STM study of close-packed monolayers under ultrahigh-vacuum conditions, *J. Phys. Chem. B*, 108 (2004) 2279–2284.
- [60] A.J. Groszek, Selective adsorption at graphite/hydrocarbon interfaces, *Proc. R. Soc. Lond. A* 314 (1970) 473–498.
- [61] G.H. Findenag, Ordered layers of aliphatic alcohols and carboxylic-acids at pure liquid-graphite interface, *J. Chem. Soc., Faraday Trans.*, 69 (1973) 1069–1078.
- [62] D.C. Parks, N.A. Clark, D.M. Walba, P.D. Beale, Scanning tunneling microscopy of coexisting 2D crystalline and 1D stacking-disordered phases at the chiral-liquid-crystal-graphite Interface, *Phys. Rev. Lett.* 70 (1993) 607–610.
- [63] D.M. Walba, F. Stevens, D.C. Parks, N.A. Clark, M.D. Wand, Near-atomic resolution imaging of ferroelectric liquid crystal molecules on graphite by STM, *Science* 267 (1995) 1144–1147.
- [64] H.F. Gong, B. Bredenkotter, C. Meier, C. Hoffmann-Richter, U. Ziener, D.G. Kurth, D. Volkmer, Self-assembly of amphiphilic hexapyridinium cations at the air/water interface and on HOPG surfaces, *ChemPhysChem* 8 (2007) 2354–2362.
- [65] B.A. Hermann, L.J. Scherer, C.E. Housecroft, E.C. Constable, Self-organized monolayers: a route to conformational switching and read-out of functional supramolecular assemblies by scanning probe methods, *Adv. Funct. Mater.* 16 (2006) 221–235.
- [66] G.M. Florio, T.L. Werblowsky, T. Mueller, B.J. Berne, G.W. Flynn, Self-assembly of small polycyclic aromatic hydrocarbons on graphite: a combined scanning tunneling microscopy and theoretical approach, *J. Phys. Chem. B* 109 (2005) 4520–4532.
- [67] M.A. Thompson, ArgusLab 4.0.1, Planaria Software LLC, Seattle, WA, USA, (2004).
- [68] H. Gawronski, J. Henzi, V. Simic-Milosevic, K. Morgenstern, Using a chemical concept for reactivity for the interpretation of STM images of physisorbed molecules, *Appl. Surf. Sci.* 253 (2007) 9047–9053.
- [69] K. Shibasaki, A. Fujii, N. Mikami, S. Suzuki, Magnitude of the CH/ π interaction in the gas phase: experimental and theoretical determination of the accurate interaction energy in benzene-methane, *J. Phys. Chem. A* 110 (2006) 4397–4404.
- [70] W. Xu, M.D. Dong, H. Gersen, E. Rauls, S. Vazquez-Campos, M. Grego-Calama, D.N. Reinhoudt, E. Lægsgaard, I. Stensgaard, T.R. Linderth, F. Besenbacher, Influence of alkyl side chains on hydrogen-bonded molecular surface nanostructures, *Small* 4 (2008) 1620–1623.
- [71] S.H. Chen, C.W. Frank, Infrared and fluorescence spectroscopic studies of self-assembled n-alkanoic acid monolayers, *Langmuir* 5 (1989) 978–987.
- [72] M. Hibino, A. Sumi, I. Hatta, Molecular arrangements of fatty acids and cholesterol at liquid/graphite interface observed by scanning tunneling microscopy, *Jpn. J. Appl. Phys.* 34 (1995) 3354–3359.
- [73] M. Hibino, A. Sumi, H. Tsuchiya, I. Hatta, Microscopic origin of the odd-even effect in monolayer of fatty acids formed on a graphite surface by scanning tunneling microscopy, *J. Phys. Chem. B* 102 (1998) 4544–4547.
- [74] M. Hibino, H. Tsuchiya, Bias voltage dependence of molecular orientation of dialkyl ketone and fatty acid alkyl ester at the liquid-graphite interface, *Appl. Surf. Sci.* 317 (2014) 803–810.
- [75] B.R. Penfold, J.C.B. White, The crystal and molecular structure of benzamide, *Acta Crystallogr.* 12 (1959) 130–135.
- [76] U. Beginn, S. Sheiko, M. Möller, Self-organization of 3,4,5-tris(octyloxy)benzamide in solution and embedding of the aggregates into methacrylate resins, *Macromol. Chem. Phys.* 201 (2000) 1008–1015.